Advances in Water Resources 144 (2020) 103684

Contents lists available at ScienceDirect

Advances in Water Resources

journal homepage: www.elsevier.com/locate/advwatres

A continuum model of unstable infiltration in porous media endowed with an entropy function

Abdelaziz Beljadid[a,b], Luis Cueto-Felgueroso[c], Ruben Juanes[a,d,*]

[a] Department of Civil and Environmental Engineering, Massachusetts Institute of Technology, Cambridge, Massachusetts, USA
[b] International Water Research Institute, Mohammed VI Polytechnic University, Green City, Morocco
[c] Department of Civil Engineering: Hydraulics, Energy and Environment, Universidad Politécnica de Madrid, Madrid, Spain
[d] Department of Earth, Atmospheric and Planetary Sciences, Massachusetts Institute of Technology, Cambridge, Massachusetts, USA

ARTICLE INFO

MSC:
00-01
99-00

Keywords:
Vadose zone
Infiltration
Gravity fingering
Entropy
Nonequilibrium thermodynamics

ABSTRACT

We propose a thermodynamic approach to modeling unsaturated flow in porous media, where the liquid saturation is understood as the state variable. The free energy functional is designed as a symmetric expansion of the traditional capillary energy density in Richards equation, therefore removing ambiguities on the interpretation of the higher-order term in the model equation. The proposed definition renders a formulation that leads naturally to an entropy function of the system, and we show that the model describes an entropy-increasing process for an isolated system.

The new formulation reproduces gravity fingering during infiltration in soil. We show that the nonlinear and singular structure of the capillary pinning function in the fourth-order term plays a fundamental role in the behavior and stability of infiltration fronts, promoting front pinning and the persistence of fingered infiltration at relatively large flux ratios.

1. Introduction

Fluid dynamics through unsaturated porous media is key in understanding the distribution of soil moisture, which in turn regulates the interactions between climate, soil and vegetation. These interactions are essential in the description of the hydrological, ecological and meteorological processes (Rodriguez-Iturbe, 2000). Many infiltration models have been developed based on a variety of empirical, conceptual and physical approaches (Buckingham, 1907; Richards, 1931; Horton, 1933; Philip, 1957; 1969), but these models generally assume stable wetting and drying fronts when the medium is homogeneous. Gravity-driven displacement of one fluid by another in porous media, however, is often subject to hydrodynamic instability, whereby fluid invasion takes the form of preferential flow paths or fingers (Sahimi, 1993; Frette et al., 1992; Méheust et al., 2002); examples include secondary oil migration in reservoir rocks (Thomas and Clouse, 1995; Meakin et al., 2000; Luo et al., 2004), and infiltration of rainfall water in dry soil (Hill and Parlange, 1972; Glass et al., 1989d; Ritsema et al., 1998).

Since the 1970s, carefully designed experiments have repeatedly shown gravity fingering during infiltration in homogeneous sands (Diment and Watson, 1985; Glass et al., 1989d; 1990; Selker et al., 1992a; 1992b; Lu et al., 1994; Bauters et al., 1998; 2000; Yao and Hendrickx, 2001; Sililo and Tellam, 2000; Flekkøy et al., 2002; Wang et al., 2004; Wei et al., 2014). The selected pattern of the phenomenon is a winner-takes-all process, in which the fastest-growing fingers channelize most of the flow, and the growth of other incipient fingers is thereby suppressed (Glass et al., 1989d; Selker et al., 1992b).

In addition to the clear evidence of the gravity fingering phenomenon in laboratory experiments, several works point to its importance also in field settings (Ritsema and Dekker, 1994b; Hendrickx and Flury, 2001). Work on water flow and infiltration in textured soils has demonstrated the potential importance of fingered flow in the field (Glass et al., 1988; Ommen et al., 1989; Liu et al., 1994; Ritsema and Dekker, 1994b; 1994a; Ritsema et al., 1996; 1998; Wang et al., 2004), including the role of water repellency as a mechanism that exacerbates it (Bauters et al., 1998; Ritsema and Dekker, 2000b; 2000a; Wang et al., 2000). The formation of fingers can significantly influence the transport of contaminants to surface and ground waters (Glass et al., 1989a) and reduces the water rechargeable area in the root zone of plants.

The stability of infiltration fronts varies with the properties of the medium and the infiltrating flux. Experimental work has shown that the fingering instability is expected to be more vigorous for coarse soils (Heijs et al., 1996), for two reasons: importance of gravity vs. capillary forces, and because the soil retention curve and unsaturated conductivity are often 'sharper' (more nonlinear) for sands than for clays.

* Corresponding author.
E-mail address: juanes@mit.edu (R. Juanes).

https://doi.org/10.1016/j.advwatres.2020.103684
Received 28 September 2019; Received in revised form 8 July 2020; Accepted 8 July 2020
Available online 10 July 2020
0309-1708/© 2020 Published by Elsevier Ltd.

Although these behaviors are observed for the soils studied, the conditions of the triggering mechanism of instability to generate preferential paths of flow are complex because of the subtle interplay between gravity and capillary effects, and the impact of the macroscopic interface at the wetting front. The other important experimental trends are related to soil-water conditions, as the initial moisture content plays a critical role in the fingering instability. It is well established that fingering is promoted when the medium is quite dry and that even relatively low water saturations lead to a compact, downward-moving wetting front (Lu et al., 1994; Bauters et al., 2000). Stable fronts are also observed in dry media when the infiltration rate is either very small or approaches the saturated conductivity (Hendrickx and Yao, 1996). In general, larger infiltration rates produce faster, thicker fingers (Glass et al., 1989d).

An important feature of gravity fingering is the presence of saturation overshoot, that is, the pile-up of water at the infiltration front—which is understood to be a prerequisite for the fingering instability in unsaturated flows (DiCarlo, 2004; Egorov et al., 2003; Nieber et al., 2005; DiCarlo, 2007; Cueto-Felgueroso and Juanes, 2009a). The classical Richards model of infiltration (Richards, 1931), along with the standard (monotonic) pressure-saturation relation, is stable in homogeneous porous media under infinitesimal and finite perturbations (Nieber et al., 2005; Fürst et al., 2009). This model is incompatible with saturation overshoot for infiltration into unsaturated homogeneous media, leads to monotonic saturation profiles, and cannot reproduce the fingering phenomenon.

Many extensions to the Richards equation have been proposed in the past few decades to develop continuum mathematical models that describe gravity-driven unsaturated flows through porous media and attempt to capture finger formation (see, e.g, Cueto-Felgueroso and Juanes, 2009a; DiCarlo, 2013; Xiong, 2014 for an overview). For example, Eliassi and Glass (2002) invoked a hold-back–pile-up (HBPU) effect to develop an extension of the Richards equation with an additional higher-order term. They proposed three mathematical representations of the HBPU effect to include hypodiffusive, hyperbolic, and mixed spatial-temporal forms. Cueto-Felgueroso and Juanes (2008, 2009a) proposed a thermodynamic approach to multiphase flows through porous media, and developed a phase field model of unsaturated flow. Their model then leads to an extension of the Richards equation that includes a new term—a fourth-order derivative in space—with a scaling linking the magnitude of this term to the other terms in the Richards equation. Several authors have studied the impact of dynamic capillary pressure on unsaturated flow patterns, concluding that the extended Richards equation including dynamic capillarity and hysteresis may also lead to saturation overshoot and flow patterns that are similar to the observed wetting front instability (see, e.g, Rätz and Schweizer, 2014; van Duijn et al., 2018; Zhuang et al., 2019b).

In this study, we adopt what we consider to be a minimum-ingredients model of unsaturated flow that is compatible with the observations of hydrodynamic instability and fingering patterns during infiltration into dry coarse soil. We do not include capillary hysteresis in our model. This is because the proposed fourth-order model can lead to fingering instabilities and finger persistence without hysteresis. While hysteresis alone (without a mechanism that leads to saturation overshoot) cannot explain the formation of gravity fingers during water infiltration in soil (Eliassi and Glass, 2001; van Duijn et al., 2004; Nieber et al., 2005; Fürst et al., 2009), including hysteresis in the capillary pressure is essential to reproduce important experimental observations of unsaturated flow. Among them is the long-term stability of the finger cores as preferential flow paths (Glass et al., 1989a; Rezanezhad et al., 2006): without hysteresis, finger widths slowly continue to increase due to lateral capillary diffusion. The other phenomenon is the unconventional water flow during horizontal redistribution due to capillary hysteresis, which may lead to persistent discontinuities across sharp saturation gradients and to flow from regions of smaller saturation towards others with larger one (Philip, 1991; Raats and van Duijn, 1995; Heinen and Raats, 1999; Pop et al., 2009; van Duijn and Mitra, 2018), which may also be attributed to multistability of the capillary energy (Cueto-Felgueroso and Juanes, 2016).The higher-order term in the proposed model and in the model based on the phase field methodology (Cueto-Felgueroso and Juanes, 2009a) is responsible for triggering the instability of the flow, the formation of saturation overshoot and gravity fingers in unsaturated flows without resorting to hysteresis. We note that hysteresis is a very real phenomenon with an important macroscopic consequences (Liu et al., 1994; Bauters et al., 1998; Spiteri and Juanes, 2006; Juanes et al., 2006) which can be incorporated in the capillary-pressure function to further improve the results. While dynamic capillary pressure is sufficient to generate a saturation overshoot in 1D, Nieber et al. (2005); DiCarlo et al. (2008); Zhuang et al. (2019a), the combined effect of dynamic capillary pressure and hysteresis is needed to produce reasonable-looking overshoot and fingering patterns (Rätz and Schweizer, 2014; Zhang and Zegeling, 2017; Zhuang et al., 2019b).

The role of nonzero contact angle on unstable flow formation in porous media has been studied experimentally (Wallach et al., 2013), and a moving-boundary approach was proposed (Brindt and Wallach, 2017), which attributes the hold-back–pile-up effect to the nonzero contact angle where water is initially prevented from invading the dry pores at the wetting front. When sufficient water piles up (saturation overshoot), the pressure increases and becomes enough to overcome the impeding pressure barrier (water-entry capillary pressure). This leads to the invasion of pores and the propagation of a sharp wetting front with a nonmonotonic saturation profile.

Here we adopt a thermodynamic approach to unsaturated flow, where the liquid saturation is understood as the state variable. We design a free energy functional as a symmetric expansion of the traditional capillary energy density (Leverett, 1941; Morrow, 1970; Aavatsmark, 1989a; 1989b; Sciarra et al., 2007; Sciarra, 2016), therefore removing ambiguities on the interpretation of the nonlocal term. Our approach is based on the phase-field methodology (Cahn and Hilliard, 1958; Cueto-Felgueroso and Juanes, 2009a) where in the formulation of the capillary energy, in addition to the terms related to Richards' equation (bulk energy), we include the energy associated with the effect of the macroscopic interface (the wetting front). This energy approach leads naturally to a nonlinear higher-order term involving a special function, which we term *capillary pinning function*, multiplying the square-gradient term. The structure of this function plays a fundamental role in the behavior of continuum models of multiphase flow in a capillary tube (Cueto-Felgueroso and Juanes, 2012; Strait et al., 2015), Hele-Shaw cell (Cueto-Felgueroso and Juanes, 2014), or thin-film flow over a substrate (Pahlavan et al., 2015).

By construction, the capillary pinning function in the model proposed here is proportional to the capillary energy density. We show that this definition renders a formulation that leads naturally to an entropy function of the system, and we prove that the model leads to an entropy-increasing process for an isolated system. We also show that the proposed model reproduces the saturation overshoot at the wetting front, the formation of gravity fingers, and the pinning behavior at the base of the infiltration front.

In Section 2, we present the derivation of the proposed model and the construction of the capillary pinning function introduced. Section 3 is devoted to the construction of the entropy function of the proposed model and the analysis of the entropy of an isolated system. Numerical simulations are performed in Section 4 to evaluate the effect of the nonlinear capillary pinning function on saturation overshoot and on the pinning behavior at the base during fingered infiltration. Finally, we provide some concluding remarks in Section 5.

2. Mathematical model

2.1. Local model: Richards equation

It is useful to first describe the thermodynamic approach as it applies to the traditional unsaturated flow equation: Richards' equation

(Richards, 1931). We start by imposing mass conservation in terms of water saturation S:

$$\frac{\partial(\rho\phi S)}{\partial t} + \nabla \cdot \mathbf{F} = 0, \tag{1}$$

and mass flux driven by a potential Π:

$$\mathbf{F} = -\rho\lambda_w(S)\nabla\Pi, \tag{2}$$

where ρ is the water density, ϕ is the medium porosity, g is the gravitational acceleration (all assumed constant), and $\lambda_w(S)$ is the water mobility,

$$\lambda_w(S) = \frac{k}{\mu}k_r(S), \tag{3}$$

where k is the medium permeability, μ is the fluid dynamic viscosity, and $k_r(S)$ is the water relative permeability, which accounts for the effect of partial saturation (Richards, 1931; Muskat and Meres, 1936; Muskat, 1949; Bear, 1972). It proves convenient to introduce the saturated hydraulic conductivity,

$$K_{\text{sat}} = \frac{\rho g k}{\mu}. \tag{4}$$

The potential is derived from the energy function $\mathcal{E}$:

$$\Pi = \frac{d\mathcal{E}}{dS}. \tag{5}$$

The energy $\mathcal{E}$ comprises gravitational and capillary energy components, $\mathcal{E} = \mathcal{E}_{\text{grav}} + \mathcal{E}_{\text{cap}}$. The gravitational component is simply

$$\mathcal{E}_{\text{grav}} = -\rho g z S, \tag{6}$$

where z is depth (in the direction of gravity). The capillary component is given by

$$\mathcal{E}_{\text{cap}} = \mathcal{E}_0 + \Psi(S) \tag{7}$$

where $\mathcal{E}_0$ is a reference energy (dependent on the elevation datum and on the surface energy of the medium when filled with water) and $\Psi(S)$ is the capillary energy function, from which the capillary pressure $P_c(S)$ is derived:

$$P_c(S) = -\frac{d\Psi}{dS}, \tag{8}$$

which can be expressed in head units as the water suction head $\psi(S)$:

$$P_c(S) = \rho g\psi(S). \tag{9}$$

We will further express the water suction head ψ using the Leverett scaling (Leverett, 1941)

$$\psi(S) = h_{\text{cap}}J(S), \qquad h_{\text{cap}} \sim \frac{\gamma\cos\theta}{\rho g\sqrt{k/\phi}}, \tag{10}$$

where h_{cap} is the characteristic capillary rise, γ is the surface tension between the fluids, θ is the contact angle, and $J(S)$ is the Leverett J-function (Leverett, 1941), which is a dimensionless version of the capillary pressure function.

Using Eqs. (8)–(10), we can write Eq. (7) as

$$\mathcal{E}_{\text{cap}} = \mathcal{E}_0 - \rho g h_{\text{cap}} I(S), \qquad I(S) = \int_0^S J(s)\,ds. \tag{11}$$

We refer to $I(S)$ as the dimensionless capillary energy density (Leverett, 1941; Morrow, 1970; Aavatsmark, 1989a; 1989b). The flow potential based on this energy is given by:

$$\Pi = \frac{d\mathcal{E}}{dS} = \rho g[-z - \psi(S)]. \tag{12}$$

Finally, inserting Eq. (12) into the flux Eq. (2) and the mass conservation Eq. (1), and assuming constant fluid density, yields the classical Richards equation:

$$\phi\frac{\partial S}{\partial t} + \nabla \cdot \left[K_{\text{sat}}k_r(S)\nabla(z + \psi(S))\right] = 0. \tag{13}$$

2.2. Nonlocal model

To develop a model capable of unstable infiltration, we propose a second gradient theory (Sciarra et al., 2007; Sciarra, 2016) of the capillary energy, written as a second-order expansion of the classical (local) one:

$$\mathcal{E}^{\nabla}_{\text{cap}} = \mathcal{E}_0 + \rho g h_{\text{cap}} I(S)\left(-1 + \frac{1}{2}\delta^2|\nabla S|^2\right), \tag{14}$$

where δ is the characteristic length scale of the diffuse interface. Written in the form of a nonlinear Cahn–Hilliard free energy (Cahn and Hilliard, 1958; Cahn, 1961; Bray, 1994; Anderson et al., 1998; Boettinger et al., 2002; Emmerich, 2008), the capillary energy includes a bulk and an interfacial contribution, which accounts for the structure of the diffuse-interface of wetting fronts:

$$\mathcal{E}^{\nabla}_{\text{cap}} = \underbrace{\mathcal{E}_0 - \rho g h_{\text{cap}} I(S)}_{\mathcal{E}_{\text{cap,bulk}}} + \underbrace{\frac{1}{2}\rho g\kappa(S)|\nabla S|^2}_{\mathcal{E}_{\text{cap,interf}}}, \tag{15}$$

where we identify κ as being the capillary pinning function

$$\kappa(S) \equiv h_{\text{cap}}\delta^2 I(S) = h_{\text{cap}}\delta^2\int_0^S J(s)\,ds. \tag{16}$$

The modified gradient-theory energy functional is $\mathcal{E}^{\nabla} = \mathcal{E}_{\text{grav}} + \mathcal{E}^{\nabla}_{\text{cap}}$. The flow potential is obtained by taking the variational derivative of the energy functional with respect to saturation, rather than the total derivative (Witelski, 1998):

$$\Pi^{\nabla} = \frac{\delta\mathcal{E}^{\nabla}}{\delta S} = \frac{\partial\mathcal{E}^{\nabla}}{\partial S} - \nabla\cdot\left(\frac{\partial\mathcal{E}^{\nabla}}{\partial\nabla S}\right) = \rho g\left[-z - \psi(S) - \sqrt{\kappa(S)}\nabla\cdot\left(\sqrt{\kappa(S)}\nabla S\right)\right], \tag{17}$$

so that conservation of mass yields the new model:

$$\phi\frac{\partial S}{\partial t} + \nabla\cdot\left[K_{\text{sat}}k_r(S)\nabla\left(z + \psi(S) + \sqrt{\kappa(S)}\nabla\cdot\left(\sqrt{\kappa(S)}\nabla S\right)\right)\right] = 0. \tag{18}$$

2.3. Capillary pressure and relative permeability functions

The capillary pressure function is typically a decreasing function of saturation (Richards, 1931; Leverett, 1941; Bear, 1972). Based on standard constitutive-relation modeling (Brooks and Corey, 1966; van Genuchten, 1980), we adopt functional forms that lead to a stable state (energy minimum) for $S < 1$ (Cueto-Felgueroso and Juanes, 2009a). We model the Leverett J-function, $J(S)$ (Leverett, 1941), as (Fig. 1b):

$$J(S) = S^{-1/\lambda}\left[1 - \exp\left(\beta\left(S - \upsilon_e\right)\right)\left(1 + \beta\frac{\lambda}{\lambda - 1}S\right)\right], \tag{19}$$

where λ is a parameter in the Brooks and Corey model (Brooks and Corey, 1966), and $\beta > 0$ and $\upsilon_{e_{\max}} > \upsilon_e \geq 1$ are parameters controlling the position of the energy minimum with $\upsilon_{e_{\max}} = 1 + \frac{1}{\beta}\ln(1 + \frac{\beta\lambda}{\lambda - 1})$ is the maximum tolerable value of υ_e to have an energy minimum for $S < 1$.

The bulk capillary energy and gradient-energy coefficient are determined by the integral of the J-function, $I(S)$, which is given by:

$$I(S) = \frac{\lambda}{\lambda - 1}S^{\frac{\lambda - 1}{\lambda}}\left[1 - \exp\left(\beta\left(S - \upsilon_e\right)\right)\right]. \tag{20}$$

The above relationship leads to convex capillary energies and nonnegative gradient-energy coefficients κ, which satisfy $\kappa(S = 0) = 0$ (Fig. 1a). The use of this type of capillary bulk energy function is motivated by the physics of infiltration: when the medium approaches full saturation ($S \approx 1$), the two assumptions of infinite mobility and infinity compressibility of air cease to be valid; therefore, the energy of the system must include an extra term due to the water pressure behind the front (Bauters et al., 1998). From a modeling perspective, the additional term introduces a steep increase in the bulk energy as $S \to 1$, preventing the saturation from taking values above 1 (Fig. 1b).

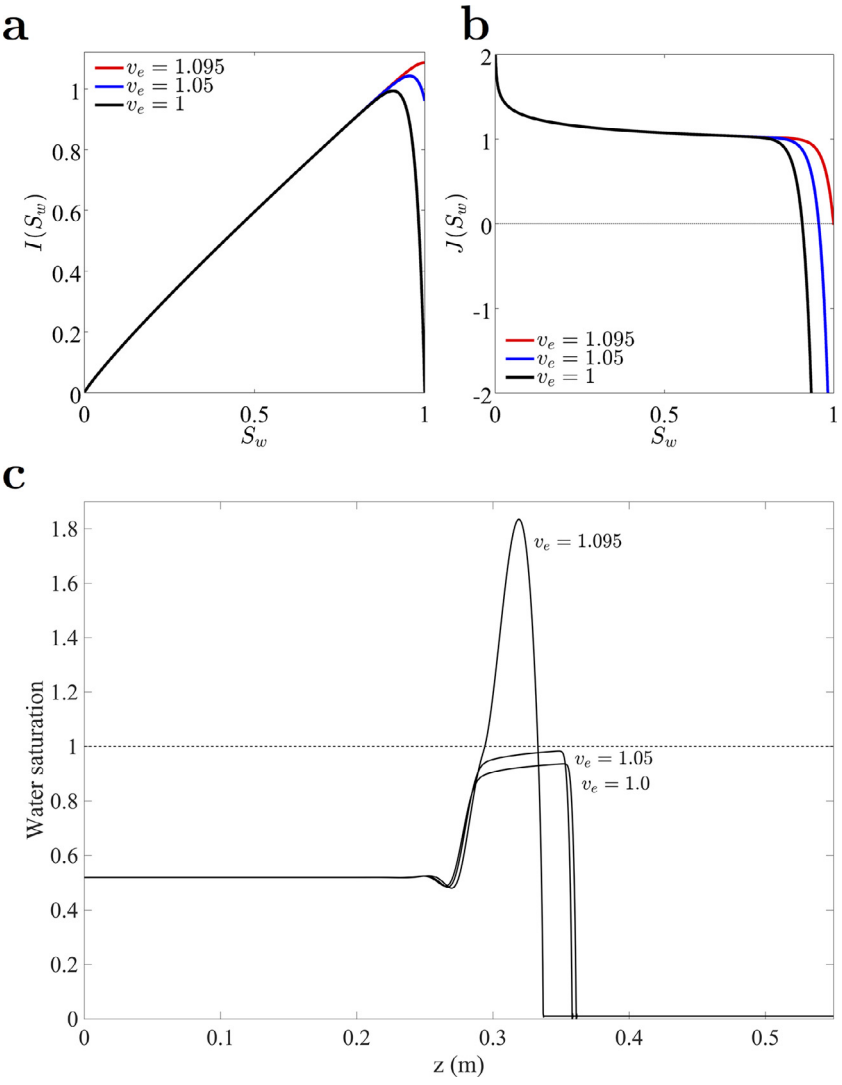

Fig. 1. **(a)** Bulk free energy I and **(b)** its derivative with respect to water saturation, $J = dI/dS$. The capillary free energy is constructed from a classical Brooks–Corey capillary pressure function, for different values of the parameter v_e. **(c)** Saturation profiles for one-dimensional infiltration with flux ratio $R_s = 0.01$, capillary height $h_{\text{cap}} = 0.02$ m, $\delta = 0.01$ m, $K_{\text{sat}} = 40$ cm/min, initial saturation is 0.01, and $v_e = 1.095, 1.05$ and 1. The latter values guarantee saturations lower than 1, while the former leads to unphysical saturations larger than 1.

In our construction of the proposed model, the use of a convex bulk capillary energy function leads to monotonic capillary pressure, which is compatible with the initial Richards equation. As will be explained in the next section, we discover that the use of a convex bulk capillary energy function and the expansion (14) for the capillary energy using the second gradient theory leads to a thermodynamically consistent model of unsaturated flow.

The only requirement that we impose on the relative permeability function $k_r(S)$ is that it be smooth and convex. Typical functional forms include those of Brooks and Corey (1966) and van Genuchten (1980). Here, we use a simple power-law relation:

$$k_r(S) = S^{\alpha}, \tag{21}$$

with $\alpha > 1$.

A simple power law in saturation $k_r(S) = S^{\alpha}$ is often used as a parsimonious approach to modeling the relative permeability function (Corey, 1954; Brooks and Corey, 1966). The exponent α can have different values for lower and higher water saturation and depending on the type of soils. Such different behaviors for the relative permeability are observed experimentally (DiCarlo, 2007; 2004). High values of the parameter α can be obtained, as shown in Cueto-Felgueroso and Juanes (2009a) to fit the experimental results in DiCarlo (2004) where the parameter α is between 2 and 11 for the types of soil considered in the study (Cueto-Felgueroso and Juanes, 2009a). This power-law behavior (with relatively large exponent) can also be seen as a smoother version of relative permeabilities with lower exponent where there is a cut-off water saturation (an irreducible water saturation).

3. Entropy function

The existence of an entropy function for a conservation law is a constructive proof that the model is well posed and thermodynamically consistent (Dafermos, 2000; LeFloch, 2002). Generally, in the process of solving systems of conservation laws one has to deal with weak solutions where uniqueness is lost. Further criteria are required, where a companion balance law should be introduced using a convex function (mathematical entropy) of the variable of the initial system to characterize the admissible (unique) solution of this system for any arbitrary initial and boundary conditions. In continuum physics, the companion balance law is intimately related with the second law of thermodynamics (Dafermos, 2000), where the variable is the physical entropy with associated entropy flux. Although some systems such as diffusion models are endowed with a rich collection of entropies, only one of them enjoys a physical interpretation. In multiphase flow, a thermodynamic approach can be used to express the Helmholtz free energy per unit pore volume (Aavatsmark, 1989a; 1989b) and determine the “natural” entropy that has a physical interpretation. To verify that this entropy function can characterize admissible solutions, the resulting differential equation using this entropy function should be integrated over an isolated system to demonstrate that the system describes an entropy-increasing process.

Here we construct the entropy function for our mathematical model of unsaturated flow, and show that it leads to an entropy-increasing evolution (positive dissipation) for an isolated system.

We start by writing the model system in 1D as follows:

$$S_t + (f(S))_z - (f(S)\Phi^{\nabla}_{\text{cap},z})_z = 0, \tag{22}$$

where subscripts indicate partial derivatives, the flux function is defined as

$$f(S) := \frac{K_{\text{sat}}}{\phi} k_r(S), \tag{23}$$

and $\Phi^{\nabla}_{\text{cap}}$ is the gradient-theory capillary potential:

$$\Phi^{\nabla}_{\text{cap}} \equiv \frac{\Pi^{\nabla}_{\text{cap}}}{\rho g} = -\psi(S) - \sqrt{\kappa(S)}\nabla \cdot \left(\sqrt{\kappa(S)}\nabla S\right). \tag{24}$$

For notational convenience, hereafter we write $\Phi := \Phi^{\nabla}_{\text{cap}}$.

In the absence of the nonlocal term, Eq. (22) has a similar form to the Buckley–Leverett equation (Buckley and Leverett, 1942), but with a convex flux function. Aavatsmark (1989a,b) studied the Buckley–Leverett equation and showed that the capillary energy density $I(S)$ is the physical entropy of the problem. For the Buckley–Leverett equation and for the Richards equation, any convex function is actually a valid entropy function due to monotonicity of the capillary pressure. This is not the case, however, for models with higher-order terms, where the definition of the entropy function usually relies on a delicate balance between diffusive and dispersive (or higher-order) terms (LeFloch, 2002).

We start by multiplying Eq. (22) by the derivative U' of a convex function of saturation $U(S)$. Assuming smooth solutions $S(z, t)$, we write:

$$U_t + (F(S))_z = U'(f(S)\Phi_z)_z, \tag{25}$$

where the entropy flux due to gravity is defined as

$$F(S) = \int_0^S U'(s)f'(s)\,ds. \tag{26}$$

To understand the influence of the right-hand-side term of Eq. (25), which includes the local effects of capillary pressure and the nonlocal effects due to saturation gradients, we analyze an isolated system in the interval $a \le z \le b$. This means that the mass flux and entropy flux (f and F, respectively) are zero at both ends of the domain. Integrating Eq. (25) in the interval $[a, b]$,

$$\frac{d}{dt}\int_a^b U\,dz + F(S)\Big|_{z=a}^{z=b} = \int_a^b U'(f\Phi_z)_z\,dz. \tag{27}$$

The second term of the left-hand side is zero because the system is isolated. We use the product rule of differentiation to write the right-hand side as:

$$\text{RHS} = \underbrace{\int_a^b \left(U'(f\Phi_z)\right)_z dz}_{=0 \text{ for isolated system}} - \int_a^b (U')_z f\Phi_z\,dz = -\int_a^b U'' S_z f\Phi_z\,dz \tag{28}$$

We define the (positive) function of saturation

$$V(S) := \frac{U''(S)f(S)}{\sqrt{\kappa(S)}}, \tag{29}$$

and the spatial function $\Sigma = \sqrt{\kappa}S_z$. With these definitions, we have $\Phi = -\psi - \sqrt{\kappa}\Sigma_z$ and, substituting in Eq. (28),

$$\begin{aligned}
\text{RHS} &= -\int_a^b V\Sigma\Phi_z\,dz \\
&= \int_a^b V\Sigma\psi_z\,dz + \int_a^b V\Sigma(\sqrt{\kappa}\Sigma_z)_z\,dz \\
&= \int_a^b V\Sigma\psi' S_z\,dz + \int_a^b \left[(V\Sigma\sqrt{\kappa}\Sigma_z)_z - (V\Sigma)_z\sqrt{\kappa}\Sigma_z\right]dz \\
&= \int_a^b V\frac{\Sigma^2}{\sqrt{\kappa}}\psi'\,dz + \int_a^b (V\Sigma\sqrt{\kappa}\Sigma_z)_z\,dz \\
&\quad - \int_a^b V(\Sigma_z)^2\sqrt{\kappa}\,dz - \int_a^b V'\Sigma\Sigma_z\sqrt{\kappa}S_z\,dz.
\end{aligned} \tag{30}$$

The first term in Eq. (30) is negative by virtue of $\psi(S) = h_{\text{cap}}J(S)$ being a monotonically decreasing function. The second term is conservative, and therefore equal to zero for an isolated system. The third term is negative because all factors in the integrand are nonnegative. The signed of the fourth term in Eq. (30) is in principle undetermined, but can be made equal to zero by imposing that the function V be constant. Thus, we choose $V \equiv V_c > 0$, which implies from Eq. (29) that

$$U'' = V_c\frac{\sqrt{\kappa(S)}}{f(S)}. \tag{31}$$

With this definition, we have that the entropy function U of the isolated system evolves according to

$$\frac{d}{dt}\int_a^b U\,dz = -\int_a^b V_c\left[\Sigma^2\left(\frac{-\psi'}{\sqrt{\kappa}}\right) + (\Sigma_z)^2\sqrt{\kappa}\right]dz \le 0. \tag{32}$$

This derivation demonstrates that the proposed model is provably dissipative, and is endowed with an entropy function.

We note that if a nonconvex double-well bulk capillary energy (Cueto-Felgueroso and Juanes, 2012) is used with the second-order expansion for the capillary energy, the first term in Eq. (30) can be nonnegative, and there is no guarantee that the overall expression necessarily takes a negative value. Finally, we conclude that a convex capillary energy leading to monotonic capillary pressure function, as already proposed for Richards equation, is more suitable to our construction of the proposed model based on the second gradient theory and the proposed capillary pinning function.

4. Numerical simulations

4.1. Finite element implementation

For computational convenience, we write the model Eq. (18) as a system of two second-order PDEs:

$$\phi\frac{\partial S}{\partial t} + \frac{\partial K_{\text{sat}}k_r(S)}{\partial z} + \nabla\cdot\left(K_{\text{sat}}k_r(S)\nabla\Xi\right) = 0, \tag{33}$$

$$\Xi = \psi(S) + \sqrt{\kappa}\nabla\cdot\left(\sqrt{\kappa}\nabla S\right). \tag{34}$$

The above mixed formulation can be compactly written in vector form as:

$$\begin{pmatrix}\phi & 0\\ 0 & 0\end{pmatrix}\frac{\partial \mathbf{u}}{\partial t} + (\nabla\cdot\mathbf{\Gamma})^T = \begin{pmatrix}0\\ \frac{\Xi-\psi}{\sqrt{\kappa}}\end{pmatrix} \tag{35}$$

where the vectors of dependent variables, $\mathbf{u}$, and fluxes, $\mathbf{\Gamma}$, are given by:

$$\mathbf{u} = \begin{pmatrix}S\\ \Xi\end{pmatrix}, \quad \mathbf{\Gamma} = \begin{pmatrix}K_{\text{sat}}k_r(S)\frac{\partial\Xi}{\partial x} & \sqrt{\kappa}\frac{\partial S}{\partial x}\\ K_{\text{sat}}k_r(S)\left(1+\frac{\partial\Xi}{\partial z}\right) & \sqrt{\kappa}\frac{\partial S}{\partial z}\end{pmatrix} \tag{36}$$

The coupled Eqs. (33)–(34) are discretized in space using a standard Galerkin finite element formulation, and advanced in time using an implicit scheme (BDF2).

For constant flow-rate infiltration we impose the water infiltration flux at the top boundary:

$$\mathcal{F} := K_{\text{sat}}k_r(S)\nabla\left[z + \psi(S) + \sqrt{\kappa(S)}\nabla\cdot\left(\sqrt{\kappa(S)}\nabla S\right)\right]\cdot\mathbf{n}\Big|_{z=0} = -R_s K_{\text{sat}}, \tag{37}$$

where R_s is the flux ratio (dimensionless), which takes a value between 0 and 1 (the minus sign indicating that it is a flux *into* the domain).

The numerical simulations of 1-D systems for saturation overshoot and 2-D systems for gravity fingering are performed, respectively in Section 4.3 and Section 4.4 using initial conditions with small perturbations near the top boundary of the domain.

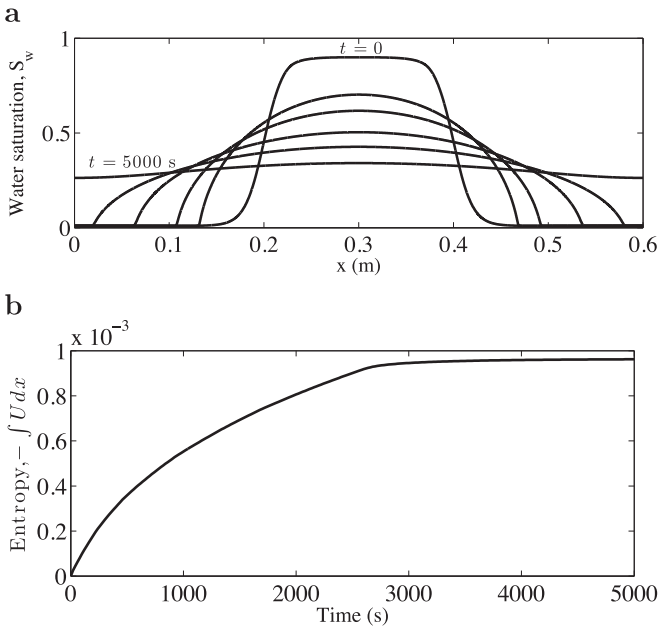

Fig. 2. Entropy production in horizontal redistribution. **(a)** Profiles of water saturation in horizontal redistribution in a closed 1D porous medium. **(b)** Evolution of the physical entropy of the system ($-\int_0^L U\,dx$), which increases monotonically in time.

4.2. Entropy production in horizontal redistribution

To test the validity of the entropy function and entropy inequality derived in Eqs. (31) and (32), we compute the evolution of the total entropy of the system, $\int U dx$ in a problem of fluid redistribution in a closed 1D horizontal porous medium of length $L = 0.6$ m (Fig. 2). The porous medium has porosity $\phi = 0.3$, saturated hydraulic conductivity $K_{\text{sat}} = 40$ cm/min, and capillary heigth $h_{\text{cap}} = 0.02$ m, and $\delta = 0.01$ m while the relative permeability function is $k_r = S^3$. We define a smooth initial saturation profile, and let the saturations redistribute with no-flow boundary conditions, so that the saturation at long times is uniform (Fig. 2a). The mathematical entropy function decreases in time. We plot the physical entropy ($-\int_0^L U\,dx$), which increases monotonically with time, demonstrating that the system is dissipative (Fig. 2b).

4.3. One-dimensional simulations of saturation overshoot

We simulate one-dimensional constant-flux infiltration into a dry porous column (Figs. 1c–3– 4). The porous medium has porosity $\phi = 0.3$, saturated hydraulic conductivity $K_{\text{sat}} = 40$ cm/min, and capillary heigth $h_{\text{cap}} = 0.02$ m, while the relative permeability function is $k_r = S^7$. We impose a water influx at the top boundary that is a fraction of the saturated conductivity, q_0, and define the flux ratio as $R_s = q_0/K_{\text{sat}}$.

We begin by exploring the role of the capillary energy function on the overshoot characteristics (Fig. 1c). In particular, we analyze whether the infiltration profiles satisfy the physical requirement that $S \leq 1$. We set a flux ratio of $R_s = 0.01$, and simulate the evolution of saturation profiles for several forms of the J-function. The bulk capillary energy is characterized by $\lambda = 10$, $\beta = 40$, and three values of υ_e, $\upsilon_e = 1$, 1.05 and 1.095 in Eq. (19). While $\upsilon_e = 1$ seems to guarantee that water saturations do not exceed 1, larger values lead to unbounded saturations for sufficiently large flux ratios and particular parameter combinations. The value of υ_e has a large influence on the magnitude of the nonlocal term. The use of $\upsilon_e = 1.095$, which is very close to the maximum tolerable value $\upsilon_{e_{\max}} \approx 1.09541$ corresponding to the parameters taken into account in the numerical test, seems to have a significant impact on the magnitude of the nonlocal term when the maximum saturation is close to the value of one. For values of υ_e which are not large, when the saturation value is in the vicinity of one, the magnitude of the nonlocal term becomes negligible compared to the other terms due to gravity and capillary pressure. As a consequence, the model equation becomes very close to Richards equation, which allows the model to respect that the computed values of water saturation remain bounded.

The most remarkable feature of the saturation profiles obtained with the proposed form of the capillary pinning function, κ, is that the saturation overshoot remains close to unity across a wide range of flux ratios (Fig. 3). The pile-up effect leads to overshoots whose length increases with flux ratio, propagating upstream from the sharp wetting front. This is consistent with experimental observations, and in contrast with choosing a constant value of κ, which yields a sharp decline of the saturation overshoot as R_s decreases (Cueto-Felgueroso and Juanes, 2009a). Because κ vanishes at $S = 0$, wetting fronts are steeper, inducing a more pronounced pile–up effect.

The length of the overshoot region is controlled by the capillary pressure function, by the flux ratio (Fig. 3), and by the strength of the gradient energy term. The latter can be characterized through the ratio between two characteristic lengths: the capillary height h_{cap}, which mathematically controls the strength of capillary diffusion, and the gradient-energy length δ, which controls the size of the energy expansion term in Eq. (14). Larger values of δ/h_{cap} increase the relative strength of the fourth-order term in the model, increasing the height and width of the overshoot (Fig. 4).

Mathematically, the saturation undershoot behind the tip of the advancing wetting front is due to the presence of the fourth-order term in the flow equation. Fourth-order diffusion allows for nonmonotonic saturations, which implies the possibility of saturation overshoot, but also the possible presence of an undershoot right above the tip. While inherent to higher-order models of unsaturated flow, this oscillatory behavior is quickly damped by the strongly dissipative fourth-order term. In contrast, oscillations are very strong in the model of unsaturated flow with dynamic capillarity (e.g., Nieber et al., 2005; Zhuang et al., 2019b). Note that the undershoot can be removed (as in the model with dynamic capillary pressure) by considering hysteresis in the capillary pressure curve (Sander et al., 2008; Zhang and Zegeling, 2017).

Rezanezhad et al. (2006), and Rezanezhad (2007) have studied the physical relevance of an undershoot behind the finger tip for the fingered flow through initially dry sand. They measured water content dynamics within the finger tip, along the finger core behind the tip, and within the fringe of the finger. The results of their experimental study revealed a saturation minimum (undershoot) behind the tip of the advancing finger (Rezanezhad et al., 2006), and the authors concluded that behind the tip of the advancing wetting front there is an additional lateral gradient which leads to a horizontal flow component. We note that, as it has already been mentioned (Sander et al., 2008), small oscillations are observed downstream of the wetting front of fingers by Glass et al. (1989c), but the authors did not comment on these observations.

In general, existing experiments are inconclusive in terms of either confirming or ruling out the undershooting phenomenon observed in higher-order models of unsaturated flow. Some of the profiles of 1D infiltration are rather oscillatory near the wetting front (Zhuang et al., 2019b, Fig. 4), and some 2D experiments actually seem to exhibit a behavior similar to the one shown in Figs. 3 and 4 (Rezanezhad et al., 2006, Fig. 9). Further experimental studies are necessary to assess whether the observed oscillations actually occur and under what conditions, or whether such behavior is instead just a mathematical property of the higher–order model, without a direct correlate in the physical system.

4.4. Two-dimensional simulations of gravity fingering

Numerical simulations are performed using the proposed model to investigate the behaviors of gravity fingers compared to experimental and theoretical results. Experimental studies are performed

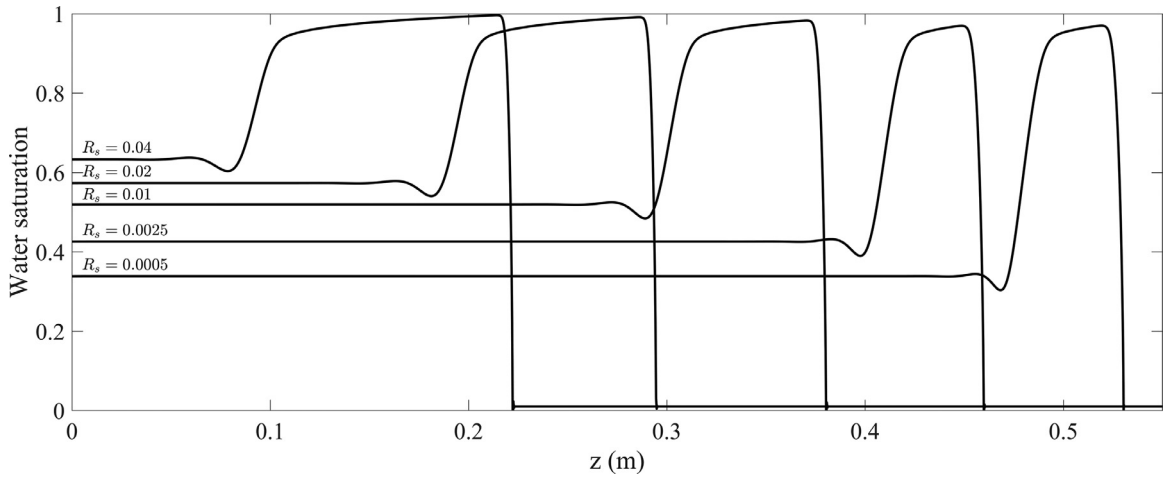

Fig. 3. Saturation profiles for one-dimensional infiltration at different flux ratios, R_s. The capillary height is $h_{\text{cap}} = 0.02$ m, $\delta = 0.01$ m, $K_{\text{sat}} = 40$ cm/min, and the initial saturation is S_0=0.01. For the capillary energy we set $\lambda = 10$, $\beta = 40$, and $\upsilon_e = 1.05$. With the proposed form of κ, the overshoot saturation remains close to unity across a wide range of flux ratios. As R_s increases, the width of the finger tip increases. The profiles are plotted at different times to allow a straightforward visual identification.

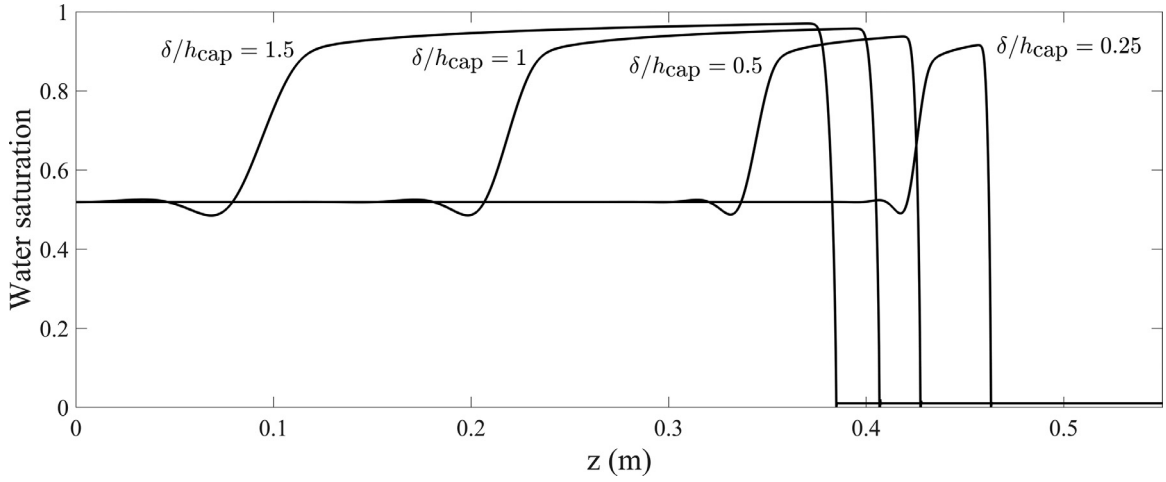

Fig. 4. Saturation profiles for one-dimensional infiltration with flux ratios, $R_s = 0.01$, capillary height $h_{\text{cap}} = 0.02$ m, $K_{\text{sat}} = 40$ cm/min, and $\delta/h_{\text{cap}} = 1.5$, 1, 0.5 and 0.25. For the capillary energy we set $\lambda = 10$, $\beta = 40$ and $\upsilon_e = 1$.

(Glass et al., 1989d) and guided by theoretical analysis (Glass et al., 1989b) for wetting front instability in porous media. These studies were applied at the finger scale and large chamber scale by imposing a constant-rate infiltration at the top boundary for various flux ratios. The results show that the number of fingers remains essentially the same as the flux ratio is increased through moderates values. At relatively large flux ratios, the number of fingers decreases and the width of fingers increases with increasing the flux ratio and ultimately tends to one large finger to cover the whole domain. The sensitivity of the model's behavior in terms of finger characteristics to the model's parameters was rather exhaustively analyzed in Cueto-Felgueroso and Juanes (2009a) for the original infiltration model with constant κ.

We simulate 2D constant-flux infiltration into a dry porous medium (Figs. 5–9). The medium properties are the same as those of the 1D simulations: porosity $\phi = 0.3$, saturated hydraulic conductivity $K_{\text{sat}} = 40$ cm/min, capillary heigth $h_{\text{cap}} = 0.02$ m, and relative permeability $k_r = S^7$. The bulk capillary energy is characterized by $\lambda = 10$, $\beta = 40$, and $\upsilon_e = 1.05$ in Eq. (19). The computational domain is a rectangle with dimensions 0.3×0.6 m^2. We impose the water flux at the top boundary, and define the flux ratio as in the 1D simulations, $R_s = q_0/K_{\text{sat}}$.

The 2D patterns of water saturation for infiltration in dry soil under different flux ratios reveal a transition from fingered to compact infiltration as R_s approaches unity (Figs. 5 and 6). This transition is consistent with experimental observations of the wetting front instability (Glass et al., 1989d). At relatively large flux ratios, the number of fingers decreases as the infiltrating flux increases, while the finger width increases with flux ratio. Furthermore, the number of fingers remains constant as the flux ratio is increased through moderates values. Our model predictions are in good agreement with the experimental observations (Glass et al., 1989d) and analysis (Glass et al., 1989b; Parlange and Hill, 1976) performed for gravity-driven fingers. The numerical simulations of the proposed model show that some of the fingers can advance faster than others, which is compatible with experimental observations of gravity-driven fingers in unsaturated media (Glass et al., 1989c; 1989d; 1989a; 1988).

The ratio of characteristic length scales δ/h_{cap}, which compares the strength of the gradient capillary energy with the capillary height, sets the finger-width scale when the other model parameters are kept constant (Fig. 7). In particular, the ratio δ/h_{cap} could be used to calibrate the model, by matching experimental observations of gravity fingering with different infiltration rates. The functional relationship developed

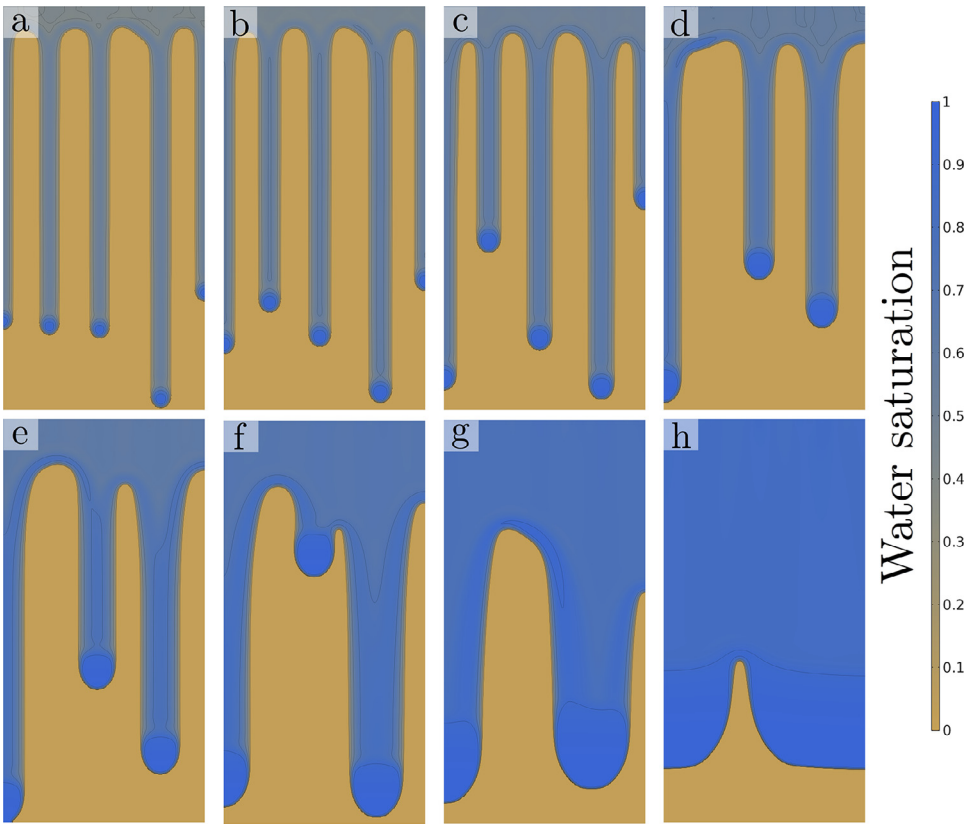

Fig. 5. Maps of water saturation for constant-rate infiltration at various flux ratios. We set h_{cap} = 0.02 m and δ/h_{cap} = 0.32. The flux ratios in panels **(a)–(h)** are, respectively, R_s = 0.0025, 0.005, 0.01, 0.02, 0.04, 0.08, 0.16, and 0.32. For the capillary energy we set $\lambda = 10$, $\beta = 40$ and $\upsilon_e = 1.05$.

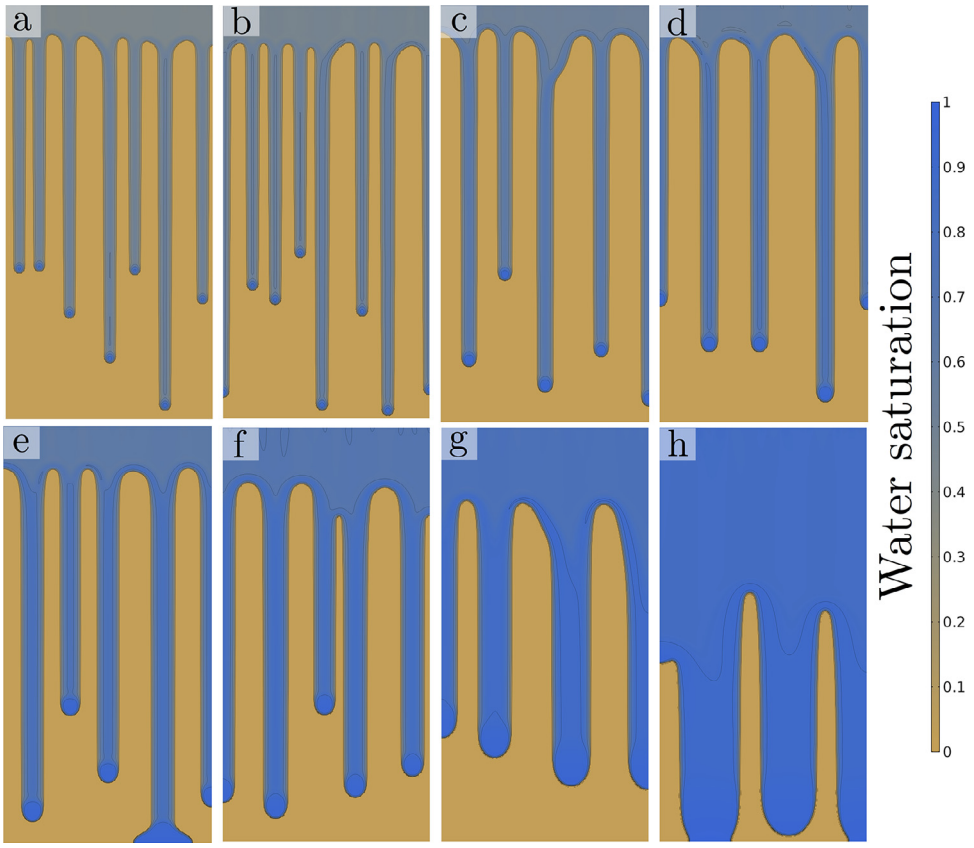

Fig. 6. Maps of water saturation for constant-rate infiltration at various flux ratios. We set h_{cap} = 0.02 m and δ/h_{cap} = 0.16. The flux ratios in panels **(a)–(h)** are, respectively, R_s = 0.0025, 0.005, 0.01, 0.02, 0.04, 0.08, 0.16, and 0.32. For the capillary energy we set $\lambda = 10$, $\beta = 40$ and $\upsilon_e = 1.05$.

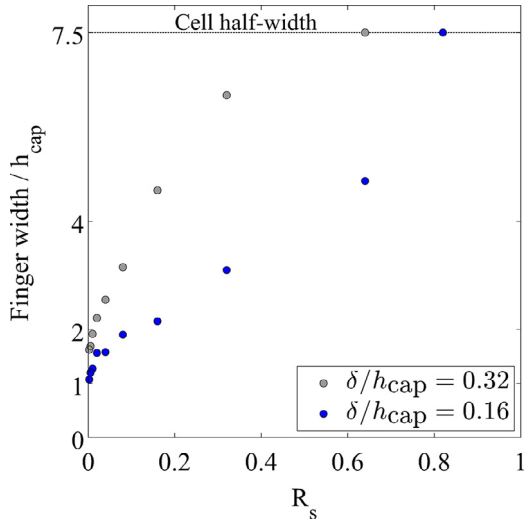

Fig. 7. Summary of average finger width as a function of flux ratio for $\delta/h_{cap} = 0.32$ and $\delta/h_{cap} = 0.16$. The capillary height is $h_{cap} = 0.02$ m.

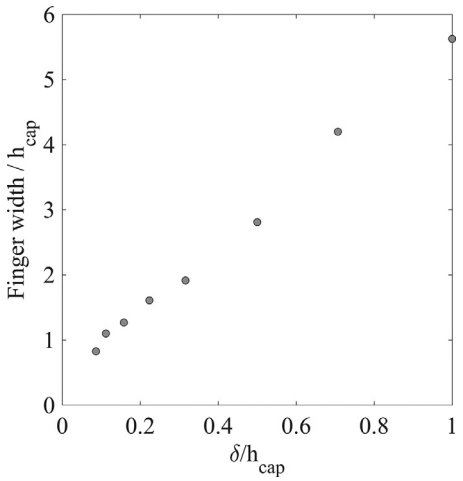

Fig. 9. Summary of average finger width as a function of δ/h_{cap} and flux ratio $R_s = 0.01$.

for the finger width (Glass et al., 1989d; 1989b; Parlange and Hill, 1976) may be fitted to experimental data and used in the calibration process of the model.

We plot the 2D saturation patterns (Fig. 8) and finger widths (Fig. 9) for infiltration at a constant infiltration flux and various values of the length scale ratio. Smaller values of δ/h_{cap} lead to thinner fingers for the same flux ratio (Figs. 8 and 9). Owing to capillary diffusion in the absence of capillary-pressure hysteresis, the fingers are also growing laterally, but this lateral growth is negligible in these simulations: the time scale for lateral growth is significantly larger than the time it takes for the fingers to reach the bottom boundary.

The experiments conducted by Yao and Hendrickx (1996) and Hendrickx and Yao (1996) demonstrated that at low flow infiltration rates the wetting fronts tend to become stable, with finger widths that increase with decreasing flux. For the present simulations in homogeneous media, decreasing infiltration rates lead to thinner fingers. This behavior makes sense from the perspective of a linear stability analysis of the model (Cueto-Felgueroso and Juanes, 2008; 2009b; 2009a). At very low rates, lateral redistribution is strong enough to prevent these thin fingers to develop, so the proposed model also leads to a stable

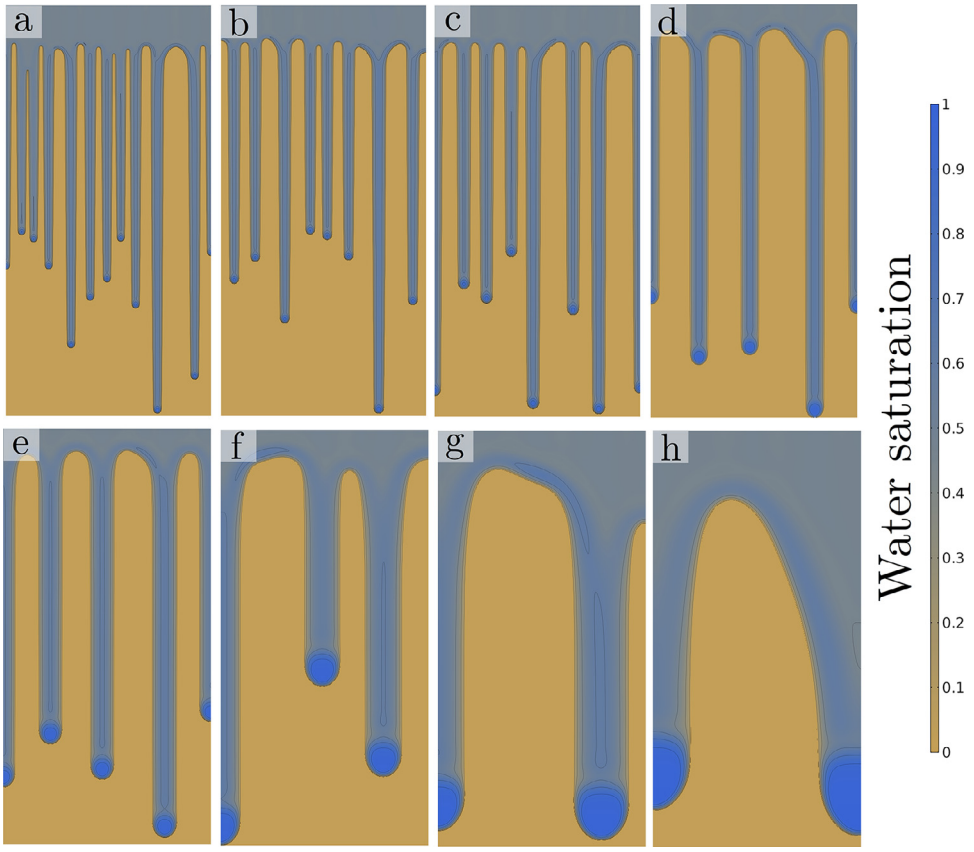

Fig. 8. Maps of water saturation for constant-rate infiltration for a fixed flux ratio of $R_s = 0.005$ and several values of δ/h_{cap}, where $h_{cap} = 0.02$ m. The length scale ratios in panels **(a)–(h)** are, respectively, $\delta/h_{cap} = 0.0866$, 0.112, 0.158, 0.224, 0.316, 0.5, 0.707, and 1. For the capillary energy we set $\lambda = 10$, $\beta = 40$ and $v_e = 1.05$.

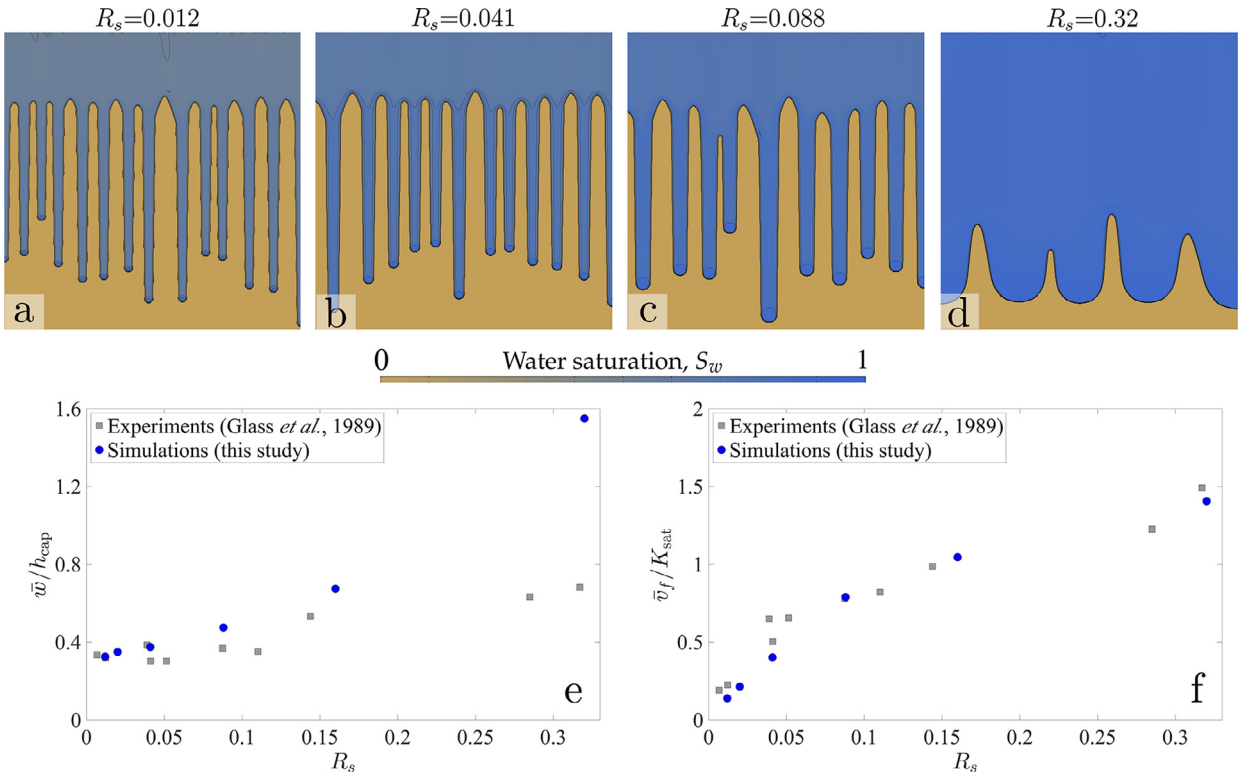

Fig. 10. Comparison between numerical simulations of fingering during water infiltration and the experiments of Glass et al. (1989d). **(a)–(d)**, Maps of water saturation for several values of the flux ratio, R_s. **(e)**, Experimental vs. numerical normalized average finger widths, w_f/h_{cap}, as a function of the flux ratio. **(f)**, Experimental vs. numerical normalized average finger speed, v_f/K_{sat}, as a function of the flux ratio.

wetting front at very low infiltration rates. A possible explanation for the discrepancy in terms of finger width at very low infiltration rates is that there is always some degree of heterogeneity in the experimental system, so that some of the very thin fingers would be suppressed, focusing the small infiltration flux towards a few ones rather than allowing the development of the natural wavelength of the instability for a homogeneous medium.

4.5. Comparison with the experiments of Glass et al. (1989)

To validate the proposed model against laboratory experiments of fingering during water infiltration, we model the experiments of Glass et al. (1989d), who studied constant-rate infiltration into packed white-silica sands. The experiments were conducted in a quasi-2D infiltration chamber, characterizing the finger morphology and dynamics over a wide range of infiltration rates, corresponding to flux ratios from $R_s = 0.01$ to $R_s = 0.82$. The sand was initially dry.

We simulate 2D constant-flux infiltration into a porous medium with very low initial saturation, $S_0 = 0.01$ (Fig. 10). We consider a square domain of dimensions 0.3×0.3 m^2, describing the experimental bottom layer composed of 14–20 sand (Glass et al., 1989d). As model parameters, we set a porosity $\phi = 0.3$, a saturated hydraulic conductivity of $K_{sat} = 40$ cm/min, a capillary heigth of $h_{cap} = 0.046$ cm, and relative permeability $k_r = S^7$. The bulk capillary energy is characterized by $\lambda = 10$, $\beta = 40$, and $v_e = 1.05$ in Eq. (19). These are the same constitutive relationships used in previous sections, which we take as representative of coarse sand. We impose the water flux at the top boundary, and free drainage at the bottom of the domain. The lateral boundaries are no-flow boundaries. To compare with the various experimental conditions, we define the flux ratio as $R_s = q_0/K_{sat}$. The computational grid is a Cartesian mesh of 600×600 finite elements.

An important step to capture the finger-width scale is to calibrate the assumed proportionality constant between δ (Eq. (14)) and h_{cap}. We fit the finger width for a small flux ratio, $R_s = 0.012$, and obtain good agreement between experimental and numerical finger width for $\delta = 0.01 h_{cap}$ for this coarse sand. We then use this relationship for all other flux ratios.

We observe good overall agreement between experiments and simulations (Fig. 10). Qualitatively, the trends of normalized finger width and finger speed are similar in experiments and in simulations (Fig. 10e and f). The agreement between observed and simulated fingers breaks down at large flux ratios: while simulations predict a transition to compact infiltration for R_s around 0.3 (Fig. 10d), experiments show persistent fingered flow up to R_s around 0.8. We attribute this discrepancy to the absence of heterogeneity and hysteresis in the model, which seems to lead to more stable infiltration patterns. We observe differences in the flow patterns at very low infiltration rates (Fig. 10a): the experiments indicate a decrease in the number of fingers, corresponding to an increase in the separation between fingers. In the simulations, the finger spacing decreases as the finger width decreases, so that more and more fingers appear in the domain. This is because the finger spacing, dictated by the characteristic wavelength of the wetting front instability, decreases with infiltration rate (Cueto-Felgueroso and Juanes, 2008, 2009a, 2009b). We attribute the discrepancy to the absence of heterogeneity in our simulations, which could suppress the growth of some fingers, focusing the small infiltration flux towards a few ones rather than allowing the development of the natural wavelength of the instability for a homogeneous medium.

5. Discussion and conclusions

In this paper, we have proposed a thermodynamic approach to modeling unsaturated flow, where the liquid saturation is understood as the state variable. The free energy functional is designed as a symmetric expansion of the traditional capillary energy density in Richards equation, therefore removing ambiguities on the interpretation of the higher-order

term in the model equation. The proposed definition renders a formulation that leads naturally to an entropy function of the system, and we show that the model describes an entropy-increasing process for an isolated system.

The new formulation of the free energy, which includes a nonlinear gradient energy through a capillary pinning function, helps identify the characteristic length scale associated with the high-order term as the finger size. More precisely, the finger width depends linearly on the ratio between gradient energy length and capillary height. The structure of this function plays a fundamental role in the behavior and stability of infiltration fronts, promoting front pinning and the persistence of fingered infiltration at relatively large flux ratios.

Comparison between simulations and experiments of fingering at various constant infiltration rates helps calibrate the relationship between the two characteristic length scales (the capillary height and the length associated with the second-gradient expansion of the capillary energy). We observe good overall agreement between experiments and simulations, deviating in the limit of nearly-saturated conditions (for which the simulations predict earlier transition to compact infiltration) and very small infiltration rates, for the experiments predict an increase of the spacing between fingers.

Our construction of the capillary pinning function provides a fundamental link between the high-order term and the traditional capillary pressure term of the unsaturated flow equation. By identifying the separate role of two characteristic length scales, namely the capillary height and the length associated with the energy expansion, the new model allows direct comparison between simulated and observed finger widths for different medium properties and infiltration fluxes. Finally, the new definition will help understand the impact of medium heterogeneity on wetting front instabilities.

Declaration of Competing Interest

The authors declare that they have no known competing financial interests or personal relationships that could have appeared to influence the work reported in this paper.

CRediT authorship contribution statement

Abdelaziz Beljadid: Investigation, Writing - original draft. **Luis Cueto-Felgueroso:** Investigation, Writing - original draft. **Ruben Juanes:** Conceptualization, Writing - review & editing.

Acknowledgments

Funding for this research was provided by the Abdul Latif Jameel World Water and Food Security Lab (J-WAFS) at MIT (to RJ). AB was supported by the Fonds de recherche du Québec – Nature et Technologies (FRQNT) and J-WAFS. LCF gratefully acknowledges funding from the Spanish Ministry of Economy and Competitiveness (grant CTM2014-54312-P). LCF and RJ also acknowledge funding from the MIT International Science and Technology Initiatives (MISTI), through a Seed Fund grant.

Supplementary material

Supplementary material associated with this article can be found, in the online version, at doi:10.1016/j.advwatres.2020.103684.

References

Raats, P.A.C., van Duijn, C.J., 1995. A note on horizontal redistribution with capillary hysteresis. Water Resour. Res. 31, 231–232.
Aavatsmark, I., 1989. Capillary energy and the entropy condition for the Buckley-Leverett equation. In: Lindquist, W.B. (Ed.), Current Progress in Hyperbolic Systems: Riemann Problems and Computations, Vol. 100 of Contemporary Mathematics. American Mathematical Society, Providence, RI, pp. 21–25.
Aavatsmark, I., 1989. Kapillarenergie als entropiefunktion. Z. Angew. Math. Mech. 69 (10), 319–327.
Anderson, D.M., McFadden, G.B., Wheeler, A.A., 1998. Diffuse-interface methods in fluid mechanics. Annu. Rev. Fluid Mech. 30, 139–165.
Bauters, T.W.J., DiCarlo, D.A., Steenhuis, T.S., Parlange, J.Y., 1998. Preferential flow in water-repellent sands. Soil Sci. Soc. Am. J. 62 (5), 1185–1190.
Bauters, T.W.J., DiCarlo, D.A., Steenhuis, T.S., Parlange, J.Y., 2000. Soil water content dependent wetting front characteristics in sands. J. Hydrol. 231, 244–254.
Bear, J., 1972. Dynamics of Fluids in Porous Media. Elsevier, New York.
Boettinger, W.J., Warren, J.A., Beckermann, C., Karma, A., 2002. Phase-field simulation of solidification. Annu. Rev. Mater. Res. 32, 163–194.
Bray, A.J., 1994. Theory of phase-ordering kinetics. Adv. Phys 43, 357–459.
Brindt, N., Wallach, R., 2017. The moving–boundary approach for modeling gravity—driven stable and unstable flow in soils. Water Resour. Res. 53, 344–360.
Brooks, R.H., Corey, A.T., 1966. Properties of porous media affecting fluid flow. J. Irrig. Drain. Div. 2, 61–88.
Buckingham, R., 1907. Studies on the movement of soil moisture. US Dept. Agr. Bur. Soils Bull. 38, 29–61.
Buckley, S.E., Leverett, M.C., 1942. Mechanism of fluid displacement in sands. Petrol. Trans. AIME 146, 107–116.
Cahn, J. W., 1961. On spinoidal decompositionActa Metall.. 9, 795–801
Cahn, J.W., Hilliard, J.E., 1958. Free energy of non-uniform systems. I. Interfacial free energy. J. Chem. Phys. 28, 258–267.
Corey, A.T., 1954. Interrelation of gas and oil relative permeabilities. Prod. Monthly 19 (1), 38–41.
Cueto-Felgueroso, L., Juanes, R., 2008. Nonlocal interface dynamics and pattern formation in gravity-driven unsaturated flow through porous media. Phys. Rev. Lett. 101, 244504. https://doi.org/10.1103/PhysRevLett.101.244504.
Cueto-Felgueroso, L., Juanes, R., 2009. A phase-field model of unsaturated flow. Water Resour. Res. 45, W10409. https://doi.org/10.1029/2009WR007945.
Cueto-Felgueroso, L., Juanes, R., 2009. Stability analysis of a phase-field model of gravity-driven unsaturated flow through porous media. Phys. Rev. E 79, 036301. https://doi.org/10.1103/PhysRevE.79.036301.
Cueto-Felgueroso, L., Juanes, R., 2012. Macroscopic phase-field modeling of partial wetting: bubbles in a capillary tube. Phys. Rev. Lett. 108, 144502. https://doi.org/10.1103/PhysRevLett.108.144502.
Cueto-Felgueroso, L., Juanes, R., 2014. A phase-field model of two-phase Hele-Shaw flow. J. Fluid Mech. 758, 522–552. https://doi.org/10.1017/jfm.2014.512.
Cueto-Felgueroso, L., Juanes, R., 2016. A discrete-domain description of multiphase flow in porous media: rugged energy landscapes and the origin of hysteresis. Geophys. Res. Lett. 43 (4), 1615–1622. https://doi.org/10.1002/2015GL067015.
Dafermos, C.M., 2000. Hyperbolic Conservation Laws in Continuum Physics. A Series of Comprehensive Studies in Mathematics, vol. 325. Springer-Verlag, Berlin.
DiCarlo, D.A., 2004. Experimental measurements of saturation overshoot on infiltration. Water Resour. Res. 40 (4), W04215. https://doi.org/10.1029/2003WR002670.
DiCarlo, D.A., 2007. Capillary pressure overshoot as a function of imbibition flux and initial water content. Water Resour. Res. 43, W08402.
DiCarlo, D.A., 2013. Stability of gravity-driven multiphase flow in porous media: 40 years of advancements. Water Resour. Res. 49 (8), 4531–4544.
DiCarlo, D.A., Juanes, R., LaForce, T., Witelski, T.P., 2008. Nonmonotonic traveling wave solutions of infiltration in porous media. Water Resour. Res. 44, W02406. https://doi.org/10.1029/2007WR005975.
Diment, G.A., Watson, K.K., 1985. Stability analysis of water movement in unsaturated porous materials 3. Experimental studies. Water Resour. Res. 21, 979–984.
van Duijn, C., Mitra, K., Pop, I., 2018. Travelling wave solutions for the Richards equation incorporating non-equilibrium effects in the capillarity pressure. Nonlinear Anal. Real World Appl. 41, 232–268.
van Duijn, C.J., Mitra, K., 2018. Hysteresis and horizontal redistribution in porous media. Transp. Porous Media 122, 375–399.
van Duijn, C.J., Pieters, G.J.M., Raats, P.A.C., 2004. Steady flows in unsaturated soils are stable. Transp. Porous Media 57, 215–244.
Egorov, A.G., Dautov, R.Z., Nieber, J.L., Sheshukov, A.Y., 2003. Stability analysis of gravity-driven infiltrating flow. Water Resour. Res. 39, 1266. https://doi.org/10.1029/2002WR001886.
Eliassi, M., Glass, R.J., 2001. On the continuum-scale modeling of gravity-driven fingers in unsaturated porous media: the inadequacy of the Richards equation with standard monotonic constitutive relations and hysteretic equations of state. Water Resour. Res. 37, 2019–2035.
Eliassi, M., Glass, R.J., 2002. On the porous-continuum modeling of gravity-driven fingers in unsaturated materials: extension of standard theory with a hold-back–pile-up effect. Water Resour. Res. 38 (11), 1234. Doi:1210.1029/2001WR001131
Emmerich, H., 2008. Advances of and by phase-field modelling in condensed matter physics. Adv. Phys. 57 (1), 1–87.
Flekkøy, E.G., Schmittbuhl, J., Løvholt, F., Oxaal, U., Måløy, K.J., Aagaard, P., 2002. Flow paths in wetting unsaturated flow: experiments and simulations. Phys. Rev. E 65, 036312.
Frette, V., Feder, J., Jøssang, T., Meakin, P., 1992. Buoyancy-driven fluid migration in porous media. Phys. Rev. Lett. 68, 3164–3167.
Fürst, T., Vodák, R., Šír, M., Bíl, M., 2009. On the incompatibility of Richards' equation and finger-like infiltration in unsaturated homogeneous porous media. Water Resour. Res. 45, W03408. https://doi.org/10.1029/2008WR007062.
van Genuchten, M.T., 1980. A closed-form equation for predicting the hydraulic conductivity of unsaturated soils. Soil Sci. Soc. Am. J. 44, 892–898.
Glass, R.J., Cann, S., King, J., Baily, N., Parlange, J.-Y., Steenhuis, T.S., 1990. Wetting front instability in unsaturated porous media: a three-dimensional study in initially dry sand. Transp. Porous Media 5, 247–268.

Glass, R.J., Oosting, G.H., Steenhuis, T.S., 1989. Preferential solute transport in layered homogeneous sands as a consequence of wetting front instability. J. Hydrol. 110 (1), 87–105.
Glass, R.J., Parlange, J.-Y., Steenhuis, T.S., 1989. Wetting front instability, 1. Theoretical discussion and dimensional analysis. Water Resour. Res. 25 (6), 1187–1194.
Glass, R.J., Steenhuis, T.S., Parlange, J., 1989. Mechanism for finger persistence in homogeneous, unsaturated, porous media: theory and verification. Soil Sci. 148, 60–70.
Glass, R.J., Steenhuis, T.S., Parlange, J.Y., 1988. Wetting front instability as a rapid and far-reaching hydrologic process in the vadose zone. J. Contam. Hydrol. 3, 207–226.
Glass, R.J., Steenhuis, T.S., Parlange, J.Y., 1989. Wetting front instability, 2. Experimental determination of relationships between system parameters and two-dimensional unstable flow field behaviour in initially dry porous media. Water Resour. Res. 25 (6), 1195–1207.
Heijs, A.W.J., Ritsema, C.J., Dekker, L.W., 1996. Three-dimensional visualization of preferential flow patterns in two soils. Geoderma 70, 101–116.
Heinen, M., Raats, P.A.C., 1999. Unconventional flow of water from dry to wet caused by hysteresis: a numerical experiment. Water Resour. Res. 35, 2587–2590.
Hendrickx, J.M.H., Flury, M., 2001. Uniform and preferential flow mechanisms in the vadose zone. In: Conceptual Models of Flow and Transport in the Fractured Vadose Zone. The National Academies Press, pp. 149–187.
Hendrickx, J.M.H., Yao, T., 1996. Prediction of wetting front stability in dry field soils using soil and precipitation data. Geoderma 70, 265–280.
Hill, D.E., Parlange, J.-Y., 1972. Wetting front instability in layered soils. Soil Sci. Soc. Am. J. 36, 697–702.
Horton, R.E., 1933. The role of infiltration in the hydrologic cycle. Trans. Am. Geophys. Union 14, 446–460.
Juanes, R., Spiteri, E.J., Orr Jr., F.M., Blunt, M.J., 2006. Impact of relative permeability hysteresis on geological CO_2 storage. Water Resour. Res. 42, W12418. https://doi.org/10.1029/2005WR004806.
LeFloch, P.G., 2002. Hyperbolic systems of conservation laws. The Theory of Classical and Nonc1assical Shock Waves. Birkhäuser Verlag, Berlin.
Leverett, M.C., 1941. Capillary behavior of porous solids. Petrol. Trans. AIME 142, 152–169.
Liu, Y., Steenhuis, T.S., Parlange, J.Y., 1994. Formation and persistence of fingered flow fields in coarse grained soils under different moisture contents. J. Hydrol. 159, 187–195.
Lu, T.X., Biggar, J.W., Nielsen, D.R., 1994. Water movement in glass bead porous media, 2. Experiments of infiltration and finger flow. Water Resour. Res. 30 (12), 3283–3290.
Luo, X., Zhang, F., Miao, S., Wang, W., Huang, Y., Zhou, B., Loggia, D., Vasseur, G., 2004. Experimental verification of oil saturation and losses during secondary migration. J. Petrol. Geol. 27 (3), 241–251.
Meakin, P., Wagner, G., Vedvik, A., Amundsen, H., Feder, J., Jøssang, T., 2000. Invasion percolation and secondary migration: experiments and simulations. Mar. Pet. Geol. 17 (7), 777–795.
Méheust, Y., Løvoll, G., Måløy, K.J., Schmittbuhl, J., 2002. Interface scaling in a two-dimensional porous medium under combined viscous, gravity, and capillary effects. Phys. Rev. E 66, 051603.
Morrow, N.R., 1970. Physics and thermodynamics of capillary action in porous media. Ind. Eng. Chem. Res. 62 (6), 32–56.
Muskat, M., 1949. Physical Principles of Oil Production. McGraw-Hill, New York.
Muskat, M., Meres, M.W., 1936. The flow of heterogeneous fluids through porous media. Physics 7, 346–363.
Nieber, J.L., Dautov, R.Z., Egorov, A.G., Sheshukov, A.Y., 2005. Dynamic capillary pressure mechanism for instability in gravity-driven flows; Review and extension to very dry conditions. Transp. Porous Media 58, 147–172.
Ommen, H.C.V., Dijksma, R., Hendrickx, J.M.H., Dekker, L.W., Hulshof, J., Heuve, M.V.D., 1989. Experimental assessment of preferential flow paths in a field soil. J. Hydrol. 105, 253–262.
Pahlavan, A.A., Cueto-Felgueroso, L., McKinley, G.H., Juanes, R., 2015. Thin films in partial wetting: internal selection of contact-line dynamics. Phys. Rev. Lett. 115, 034502. https://doi.org/10.1103/PhysRevLett.115.034502.
Parlange, J.-Y., Hill, D.E., 1976. Theoretical analysis of wetting front instability in soils. Soil Sci. 122, 236–239.
Philip, J.R., 1957. The theory of infiltration 1. The infiltration equation and its solution. Soil Sci. 83, 345–357.
Philip, J.R., 1969. Theory of infiltration. In: Chow, V.T. (Ed.), Advances in Hydroscience. Academic Press, New York, pp. 215–296.
Philip, J.R., 1991. Horizontal redistribution with capillary hysteresis. Water Resour. Res. 27, 1459–1469.
Pop, I., Duijn, C.V., Niessner, J., Hassanizadeh, S., 2009. Horizontal redistribution of fluids in a porous medium: the role of interfacial area in modeling hysteresis. Adv. Water Resour. 32 (3), 383–390.
Rätz, A., Schweizer, B., 2014. Hysteresis models and gravity fingering in porous media. 94, 645–654
Rezanezhad, F., 2007. Experimental study of fingering flow in porous hele-shaw cells. PhD Dissertation, Ruperto-Carola University of Heidelberg, Germany.
Rezanezhad, F., Vogel, H.-J., Roth, K., 2006. Experimental study of fingered flow through initially dry sand. Hydrol. Earth Syst. Sci. Discuss. 3, 2595–2620.
Richards, L.A., 1931. Capillary conduction of liquids through porous mediums. Physics 1, 318–333.
Ritsema, C.J., Dekker, L.W., 1994. How water moves in a water repellent sandy soil 2. Dynamics of fingered flow. Water Resour. Res. 9, 2519–2531.
Ritsema, C.J., Dekker, L.W., 1994. Soil moisture and dry bulk density patterns in bare dune sands. J. Hydrol. 154, 107–131.
Ritsema, C.J., Dekker, L.W., 2000. Preferential flow in water repellent sandy soils: principles and modeling implications. J. Hydrol. 231, 308–319.
Ritsema, C.J., Dekker, L.W., 2000. Wetting patterns and moisture variability in water repellent Dutch soils. J. Hydrol. 231, 148–164.
Ritsema, C.J., Dekker, L.W., Nieber, J.L., Steenhuis, T.S., 1998. Modeling and field evidence of finger formation and finger recurrence in a water repellent sandy soil. Water Resour. Res. 34 (4), 555–567.
Ritsema, C.J., Steenhuis, T.S., Parlange, J.-Y., Dekker, L.W., 1996. Predicted and observed finger diameters in field soils. Geoderma 70, 185–196.
Rodriguez-Iturbe, I., 2000. Ecohydrology: a hydrologic perspective of climate-soil-vegetation dynamics. Water Resour. Res. 36, 3–9.
Sahimi, M., 1993. Flow phenomena in rocks – from continuum models to fractals, percolation, cellular-automata, and simulated annealing. Rev. Mod. Phys. 65 (4), 1393–1534.
Sander, G.C., Glidewell, O.J., Norbury, J., 2008. Dynamic capillary pressure, hysteresis and gravity-driven fingering in porous media. J. Phys. 138, 012023.
Sciarra, G., 2016. Phase field modeling of partially saturated deformable porous media. J. Mech. Phys. Solids 94, 230–256.
Sciarra, G., dell'Isola, F., Coussy, O., 2007. Second gradient poromechanics. Int. J. Solids Struct. 44 (20), 6607–6629.
Selker, J.S., Leclerq, P., Parlange, J.-Y., Steenhuis, T., 1992. Fingered flow in two dimensions, 1. Measurement of matric potential. Water Resour. Res. 28 (9), 2513–2521.
Selker, J.S., Parlange, J.-Y., Steenhuis, T., 1992. Fingered flow in two dimensions, 2. Predicting finger moisture profile. Water Resour. Res. 28 (9), 2523–2528.
Sililo, O.T.N., Tellam, J.H., 2000. Fingering in unsaturated zone flow: a qualitative review with laboratory experiments in heterogeneous systems. Ground Water 38, 864–871.
Spiteri, E.J., Juanes, R., 2006. Impact of relative permeability hysteresis on the numerical simulation of WAG injection. J. Pet. Sci. Eng. 50 (2), 115–139.
Strait, M., Shearer, M., Levy, R., Cueto-Felgueroso, L., Juanes, R., 2015. Two fluid flow in a capillary tube. In: Springer Proceedings in Mathematics & Statistics, Vol. 109, pp. 149–161.
Thomas, M.M., Clouse, J.A., 1995. Scaled physical model of secondary oil migration. AAPG Bull. 79 (1), 19–28.
Wallach, R., Margolis, M., Graber, E.R., 2013. The role of contact angle on unstable flow formation during infiltration and drainage in wettable porous media. Water Resour. Res. 49, 6508–6521.
Wang, Z., Jury, W.A., Tuli, A., Kim, D.J., 2004. Unstable flow during redistribution: controlling factors and practical implications. Vadose Zone J. 3, 549–559.
Wang, Z., Wu, Q.J., Wu, L., Ritsema, C.J., Dekker, L.W., Feyen, J., 2000. Effects of soil water repellency on infiltration rate and flow instability. J. Hydrol. 231, 265–276.
Wei, Y., Cejas, C.M., Barrois, R., Dreyfus, R., Durian, D.J., 2014. Morphology of rain water channeling in systematically varied model sandy soils. Phys. Rev. Appl. 2, 044004.
Witelski, T.P., 1998. Equilibrium interface solutions of a degenerate singular Cahn–Hilliard equation. Appl. Math. Lett. 11 (5), 127–133.
Xiong, Y., 2014. Flow of water in porous media with saturation overshoot. A review. J. Hydrol. 510, 353–362.
Yao, T., Hendrickx, J.M.H., 1996. Stability of wetting fronts in dry homogeneous soils under low infiltration rates. Soil Sci. Soc. Am. J. 60 (1), 20–28.
Yao, T., Hendrickx, J.M.H., 2001. Stability analysis of the unsaturated water flow equation 2. Experimental verification. Water Resour. Res. 37 (7), 1875–1881.
Zhang, H., Zegeling, P., 2017. A numerical study of two-phase flow models with dynamic capillary pressure and hysteresis. Transp. Porous Media 116 (2), 825–846.
Zhuang, L., van Duijn, C., Hassanizadeh, S., 2019. The effect of dynamic capillarity in modeling saturation overshoot during infiltration. Vadose Zone J. 18 (1), 180133.
Zhuang, L., Hassanizadeh, S., van Duijn, C., Zimmermann, S., Zizina, I., Helmig, R., 2019. Experimental and numerical studies of saturation overshoot during infiltration into a dry soil. Vadose Zone J. 18 (1), 180167.